Anode Distance Effect on Field Electron Emission from Carbon Nanotubes: A Molecular/Quantum Mechanical Simulation

Chunshan He, Weiliang Wang, Shaozhi Deng, Ningsheng Xu, and Zhibing Li*

State Key Laboratory of Optoelectronic Materials and Technologies, School of Physics and Engineering, Sun Yat-sen University, Guangzhou, 510275, People's Republic of China

Guihua Chen

Dongguang University of Technology, Guangdong Dongguang, 523808, People's Republic of China

Jie Peng

Max-Planck Institute for Solid State Research, D-70569 Stuttgart, Germany

Received: November 18, 2008; Revised Manuscript Received: April 18, 2009

Field electron emission from single-walled (5,5) carbon nanotubes was simulated with a quantum chemistry method, emphasizing the effect of distance between the anode and apex. The emission probability and the field enhancement factor were obtained for different anode−apex separations with two representative applied macroscopic fields. The quantum chemistry simulation was compared to the classical finite element calculation. It was found that the field enhancement factor was overestimated by about a factor 2 in the classical calculation (for the capped carbon nanotube). The effective work function lowering due to the field penetration into the apex has important contribution to the emission probability. A peculiar decrease of the effective work function with the anode−apex separation was found for the capped carbon nanotube, and its quantum mechanical origin is discussed.

I. Introduction

Excellent field electron emission (FE) property of carbon nanotubes (CNTs) has been observed experimentally. It has shown a number of potential applications such as in flat panel displays,[1] miniature high brightness electron sources for electron microscopy,[2] parallel e-beam lithography systems, and the scanning tunneling microscopy (STM).[3,4] Generally people believe that the high aspect ratio of the CNT would lead to a great enhancement of local electric field near the apex, which would significantly reduce the thickness of the electron potential energy barrier between the CNT and the vacuum (hereafter, simply named as "the barrier") and thereby favor electron emission. In most setups for FE, the distance between the emitter and anode is large so that the finite distance effect can be ignored. However, as the longitudinal length of an emitter made of CNTs is of order of micrometers that could be comparable or even larger than the distance between the apex and anode, the location of the anode relative to the apex would have significant influence on the FE process. For application in STM, or in the future possible integrated devices with built in FE function, the anode−apex distance should be important.

Recently, some research had been done on the effect of anode location on the FE properties. Smith et al.[5,6] studied the effect of anode−cathode distance in a modified scanning electron microscope based on a parallel plate configuration model, assuming the emitter is a single-walled capped nanotube. Their results show that as the separation of the CNT to the anode increases, the threshold macroscopic field decreases and the field enhancement factor (FEF) increases asymptotically. Xu et al.[7] studied the geometrical enhancement of the FE of an individual CNT. In their setup, an etched tungsten needle with a CNT fixed on the end serves as the cathode and a melted gold wire with a ball-shaped end as the anode. Their experimental results show that the FEF increases linearly with the anode separations, while the theoretical calculations show that the nanotube length has little influence on the FEF. A tip-flat model was proposed to explain this phenomenon. In fact, the FEF depends on the atomic structure, such as open or closed cap and single-walled or multiwalled.[8−13] Recent research has shown that the FEF increases in the hydrogen-terminated open single-walled carbon nanotube (SWCNT) but decreases in the capped SWCNT, as the applied macroscopic field increases.[14]

Most of the previous theoretical studies on the effect of anode distance were based on classical models. Usually, the finite element method (FEM) was used. But the classical approach is not appropriate to deal with the electron structure in nanoscale in principle. For instance, it is difficult to define the thickness of an open SWCNT classically. When the anode approaches the nanotube, the image potential of the anode will cause electron redistribution in the CNT. Therefore the barrier and the tunneling probability will be affected. The purpose of the present paper is to investigate the quantum effect of the anode distance on the potential energy barrier quantitatively and to show the quantum contribution via the comparison of the quantum mechanical results with the classical estimation.

In order to clarify the effect of the electron redistribution caused by finite anode distance, the present paper should make use of a molecular/quantum mechanical hybrid method,[15−17] which is capable of describing the charge distribution in large scale while the electron structure at the tip is dealt with quantum mechanically. To be specific, (5,5) type single-walled carbon nanotubes (SWCNTs) were considered. The end of the SWCNT

* Corresponding author, stslzb@mail.sysu.edu.cn.

10.1021/jp810212g CCC: $40.75
Published on Web 05/29/2009

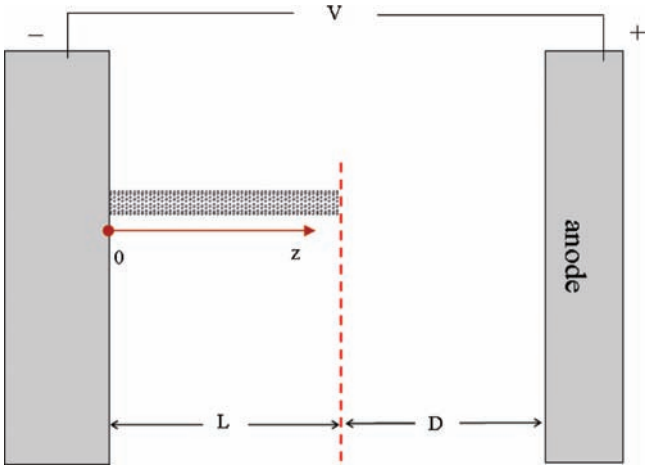

Figure 1. Setup for field electron emission of a SWCNT. The SWCNT is vertically mounted on the metal substrate (left).

is either open or capped. If the end is open, it is saturated by hydrogen atoms presumably.

In section II, the simulation method is described briefly. The calculated barrier, the FEF, and the FE probability are given in the section III. Section IV is the summary.

II. Simulation Method

Figure 1 shows the ideal setup for FE, where the SWCNT is mounted vertically on the metal substrate (cathode). The distance between the anode and apex is denoted by D. The length of the SWCNT is L. When a voltage is applied between the cathode and anode, a macroscopically uniform electrostatic field along the direction of the axis of the SWCNT is built up in the space between the cathode and anode. The existence of the SWCNT will change the electrostatic field locally and in the vicinity of the nanotube. It is expected that the field at the apex is greatly enhanced. Therefore the barrier between the apex and vacuum becomes finite and the electrons have opportunity to emit into the vacuum through the barrier by quantum tunneling. Since the tunneling probability is extremely sensitive to the barrier, the apex of the SWCNT should be treated by quantum mechanics. On the other hand, the part of the CNT on the substrate side mainly affects the tunneling probability through Coulomb interaction, so it could be described by a semiclassical method where the excess charges are treated as point charges. Then the SWCNT is divided into quantum region and semiclassical region. The size of the quantum region is yet much larger than that appropriated for standard ab initio methods. We adopted the linear scaling algorithm of Zheng et al.[15] to simulate this problem. The key point is to divide the quantum region into subregions. Each subregion and its adjacent subregion(s) form a subsystem that is simulated by the modified neglect of diatomic overlap (MNDO)[18] semiempirical quantum mechanical method. The electron density of the quantum region was calculated by Yang's divide-and-conquer method.[19] A table-searching acceleration algorithm was used.[20] The coupling of quantum region and semiclassical region was implemented

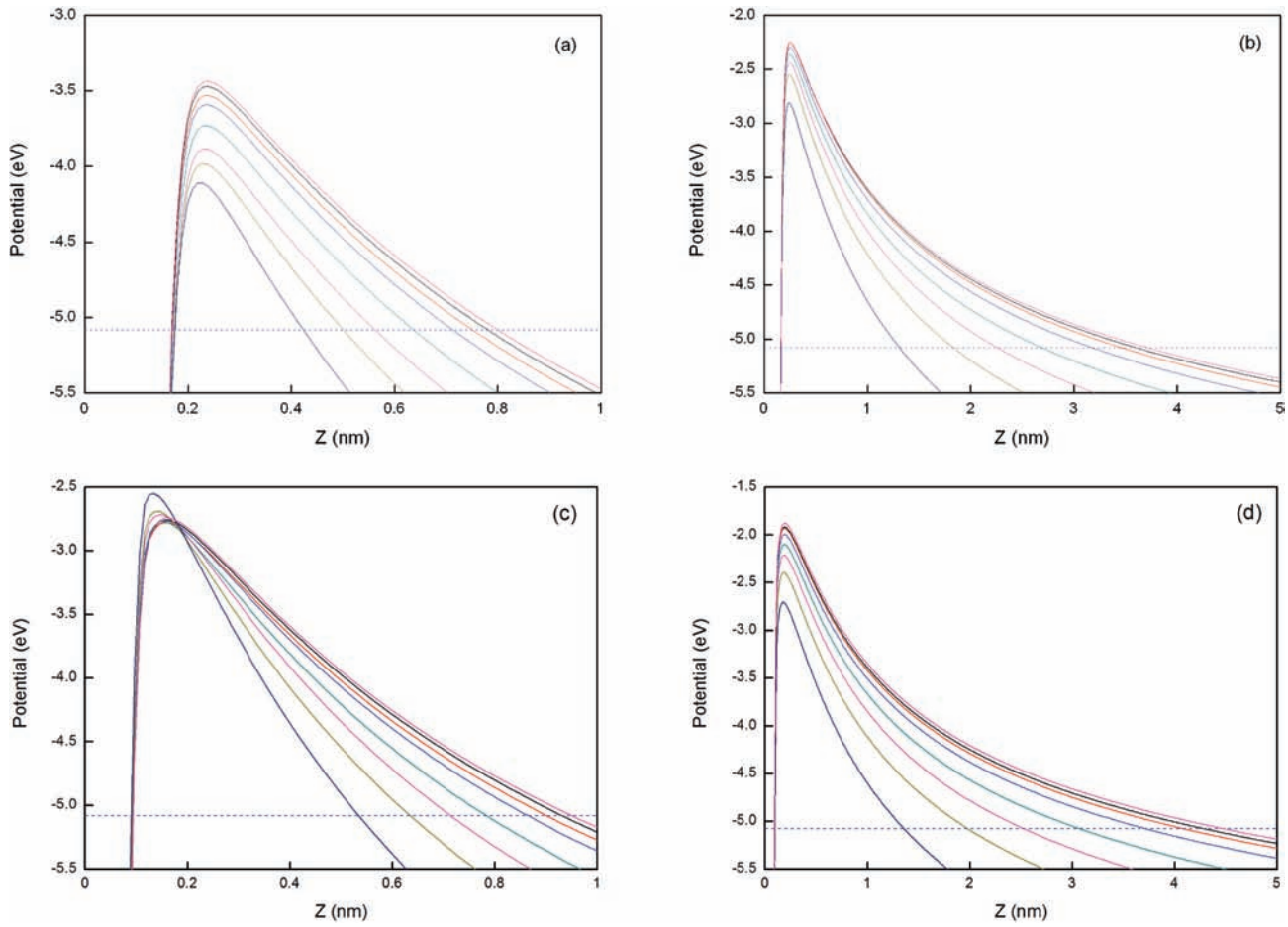

Figure 2. The potential energy barriers between the apex of (5,5) SWCNTs and vacuum. The curve of widest thickness is for the anode separated infinitely from the SWCNT. The others in the order of thickness correspond to D = 1.0, 0.5, 0.25, 0.1, 0.05, 0.025, and 0.01 μm, respectively. The dotted line is the Fermi level at −5.08 eV. (a) The open SWCNT for E = 12.0 V/μm. (b) The open SWCNT for E = 8.0 V/μm. (c) The capped SWCNT for E = 12.0 V/μm. (d) The capped SWCNT for E = V/8.0 μm.

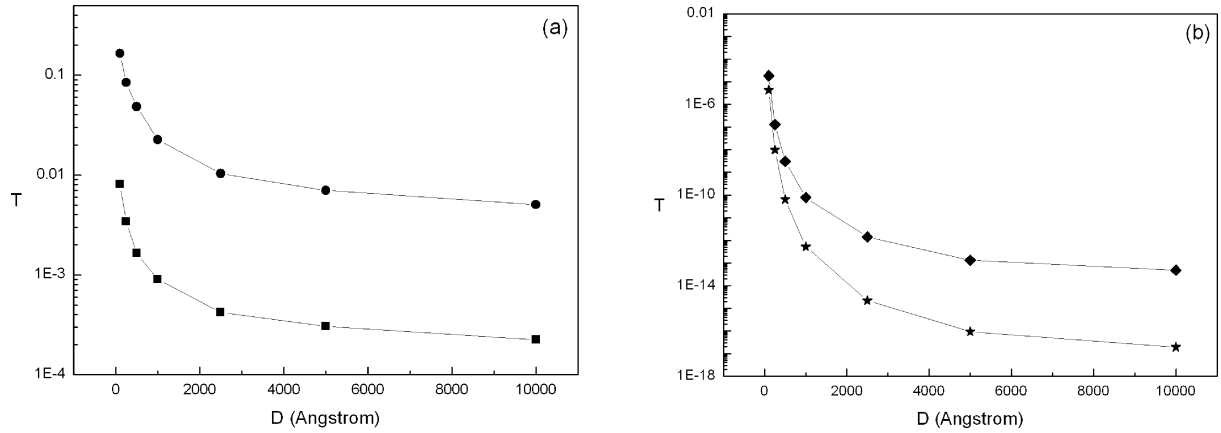

Figure 3. Field emission probability T vs anode distance D: (a) circles, open SWCNT in $E = 12.0$ V/μm; squares, capped SWCNT in $E = 12.0$ V/μm; (b) diamonds, open SWCNT in $E = 8.0$ V/μm; stars, capped SWCNT in $E = 8.0$ V/μm.

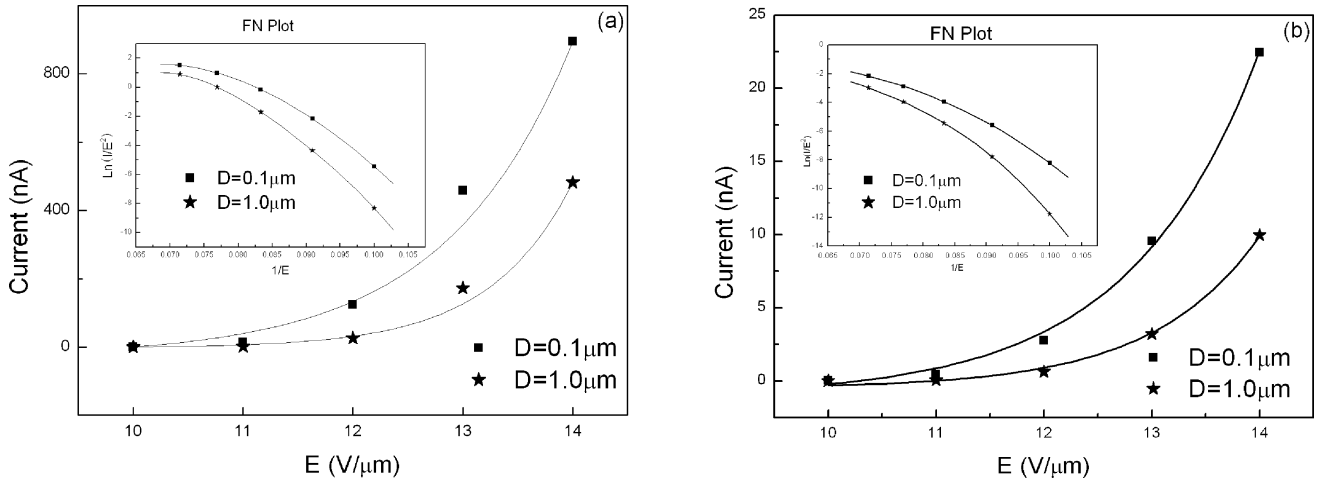

Figure 4. The FE currents vs applied macroscopic fields: squares, $D = 0.1$ μm; stars, $D = 1.0$ μm; (a) open SWCNT; (b) capped SWCNT. The insets are the FN plots.

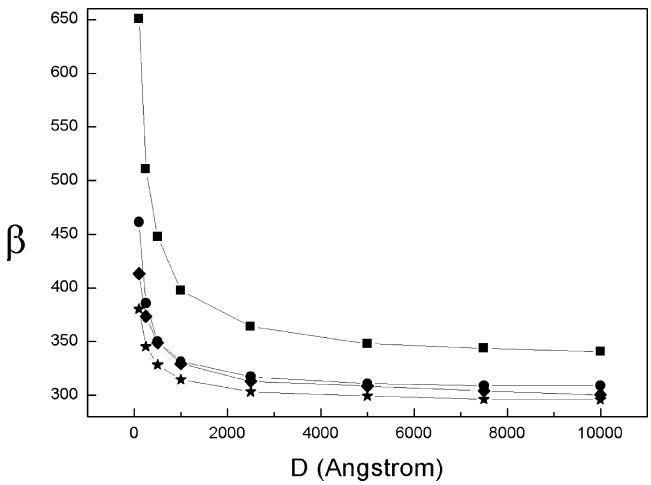

Figure 5. The field enhancement factor β vs the anode distance D: squares, capped SWCNT, $E = 12.0$ V/μm; circles, open SWCNT, $E = 12.0$ V/μm; diamonds, open SWCNT $E = 8.0$ V/μm; stars, capped SWCNT $E = 8.0$ V/μm.

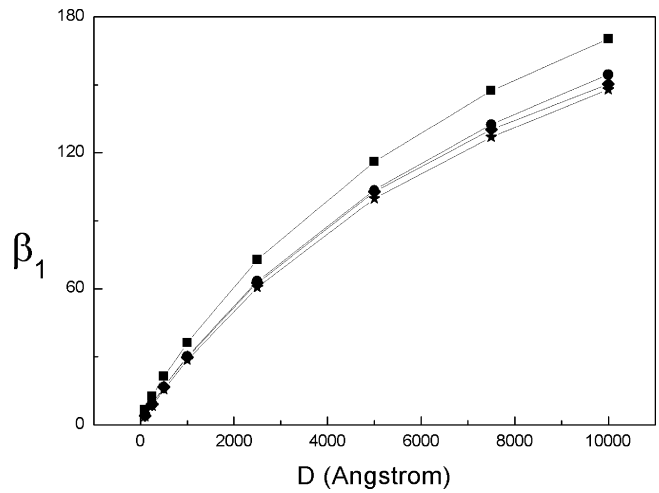

Figure 6. The field enhancement factor β_1 (as defined in ref 5) vs the anode distance D: squares, capped SWCNT, $E = 12.0$ V/μm; circles, open SWCNT, $E = 12.0$ V/μm; diamonds, open SWCNT $E = 8.0$ V/μm; stars, capped SWCNT $E = 8.0$ V/μm.

through the quasi-thermodynamic equilibrium condition, which requires a constant chemical potential (Fermi level) in the entire tube. The Fermi level E_f is below the vacuum potential in the absence of applied macroscopic field by the work function of the SWCNT, which is 5.08 eV in our simulation. In the experiment of ref 7, the substrate is made of tungsten whose work function is 4.5 eV. Hence a Schottky junction will be formed at the SWCNT−substrate connection. To avoid the complexity that arose from the Schottky junction, we assumed that the Fermi level of the SWCNT is aligned with that of the substrate.

The total field acting on the SWCNT depends on the voltage between the anode and cathode and on the charges in the SWCNT. The charges in the SWCNT induce image charges

TABLE 1: Field Enhancement Factor β (β_1) versus D, in Fixed $E = 12.0$ V/μm[a]

ending type		0.01 μm	0.025 μm	0.05 μm	0.1 μm	0.25 μm	0.5 μm	1.0 μm
open	FEM β	774.08	688.70	647.61	619.45	599.51	595.70	594.49
	quan β	484.65	416.67	379.57	349.85	327.34	317.15	311.41
	FEM E_s/E_1	7.66	16.80	30.84	56.31	119.90	198.57	297.24
	quan β_1	4.80	10.16	18.07	31.80	65.47	105.72	155.70
capped	FEM β	1132.98	978.16	909.91	873.51	848.43	840.77	834.21
	quan β	650.93	510.73	447.60	397.73	364.18	348.00	340.63
	FEM E_s/E_1	11.22	23.86	43.33	79.41	169.69	280.26	417.10
	quan β_1	6.44	12.46	21.31	36.16	72.84	116.00	170.32

[a] Where $\beta = E_s/E$ and $\beta_1 = E_s/E_1$, with E_s the local field on the apex (see the text). Entries labeled with FEM (quan) are calculated via the Finite Element Method (Quantum Chemical Simulation).

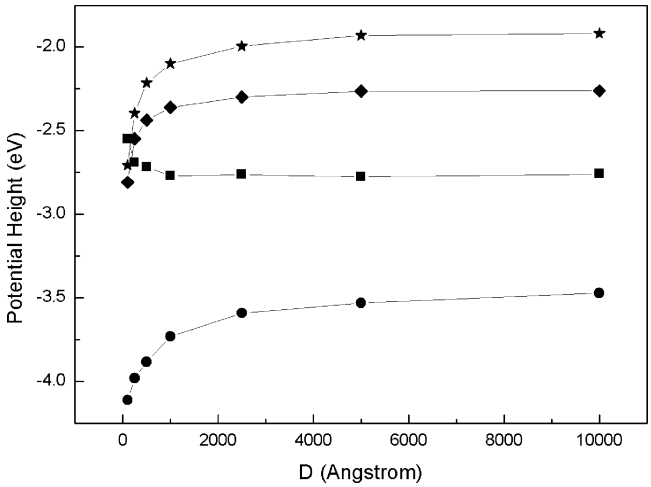

Figure 7. Potential height vs the anode distance D: stars, capped SWCNT, $E = 8.0$ V/μm; diamonds, open SWCNT, $E = 8.0$ V/μm; squares, capped SWCNT, $E = 12.0$ V/μm; circles, open SWCNT, $E = 12.0$ V/μm.

both in the cathode and in the anode. Therefore, the total field has three sources: (1) the applied macroscopic uniform field; (2) the fields of charges in the SWCNT; (3) the fields of the image charges in cathode and anode. In principle, a point charge in between two metal plates will have an infinite series of image charges. But practically, one only needs to consider the first two levels of the image charges, i.e., two images of the point charge with respect to two metal plates (the first level image charges) and the image of the first level image charge on the opposite metal plate. At the closest distance of interest here, i.e., $D = 0.01$ μm, inclusion of higher level images makes about a 0.01% difference to the predicted apex field.

Our simulation has the following steps: (1) for a given charge distribution along the tube (as an initial input), calculate the electrostatic field of the charges and the image charges; (2) simulate the SWCNT under the superposition of the applied macroscopic field and the fields calculated in the first step, to obtain a new charge distribution in the SWCNT; (3) use the new charge distribution of the second step as input, repeat the calculations through the first to the second steps, until the consistent criterion fulfilled. The consistent criterion is that the charge distribution obtained in the final step is close to the charge distribution of the previous step, with the difference less than 1.0×10^{-4} electron charge per subsystem.

The barrier between the apex and vacuum had been assumed to be the superposition of electrostatic potentials of the applied voltage, of the core ions, of valence electrons and the induced electrons in the SWCNT, and of their image charges in the metal plates. The emission probability is calculated in the JWKB approximation.[21]

III. Simulation Results

We simulated the armchair (5,5) open-ended and capped SWCNT of typical length $L = 1.0$ μm. The apex of the open-ended SWCNT is saturated by hydrogen atoms. For the (5,5) SWCNT, the radius is $r = 3.44$ Å. The applied macroscopic fields (E) ranged from 8.0 to 15.0 V/μm and various distances (D) from 10.0 nm to 1.0 μm had been investigated. In our simulation, the applied macroscopic field had been defined as

$$E = \frac{V}{L + D} \tag{1}$$

where V is the applied voltage between the anode and cathode.

A. Apex−Vacuum Barrier. The potential energy barrier between the apex and vacuum is presented in Figure 2 ((a) and (b) for the open SWCNT; (c) and (d) for the capped SWCNT). For the open SWCNT, the horizontal axis (Z axis) has the origin at a hydrogen atom of the tube end and is parallel to the tube. For the capped SWCNT, the Z axis has the origin at a carbon of the pentagon on the top. The vertical axis is the electron potential energy. The curve of widest thickness corresponds to infinite D where the distance of the anode has no effect. The others in the order of thickness correspond to $D = 1.0$, 0.5, 0.25, 0.1, 0.05, 0.025, and 0.01 μm, respectively. The dashed horizontal line indicates the Fermi level of the SWCNT. The applied macroscopic field for Figure 2a,c is $E = 12.0$ V/μm, for Figure 2b,d is $E = 8.0$ V/μm.

It is found that the potential shape changes with the variation of the anode distance. The thickness of the barrier is decreasing with D monotonously. The nonlinear change of the barrier height (especially that of the capped SWCNT in 12.0 V/μm) is remarkable. According to the tunneling theory, both lowering and narrowing of the barrier will cause significant increase of FE probability. The numerical results of the emission probability are given in the next subsection B. The thickness of the barrier and the height of the barrier will be discussed in subsections C and D, respectively.

B. Characteristic Emission Probability. It is known that the barrier in the circumambience of the SWCNT is high and thick;[14] therefore electrons would most probably emit forward from the first layer of atoms of the apex. The transmission coefficient (T) can be estimated by the JWKB approximation

$$T = \exp\left[-\frac{2}{\hbar}\int \sqrt{2m[U(z) - E_f]}\, dz\right] \tag{2}$$

where $U(z)$ is the electron potential energy, E_f is the Fermi level, and the integral is over the classical forbidden region ($U(z) - E_f > 0$). It is the characteristic emission probability (hereafter

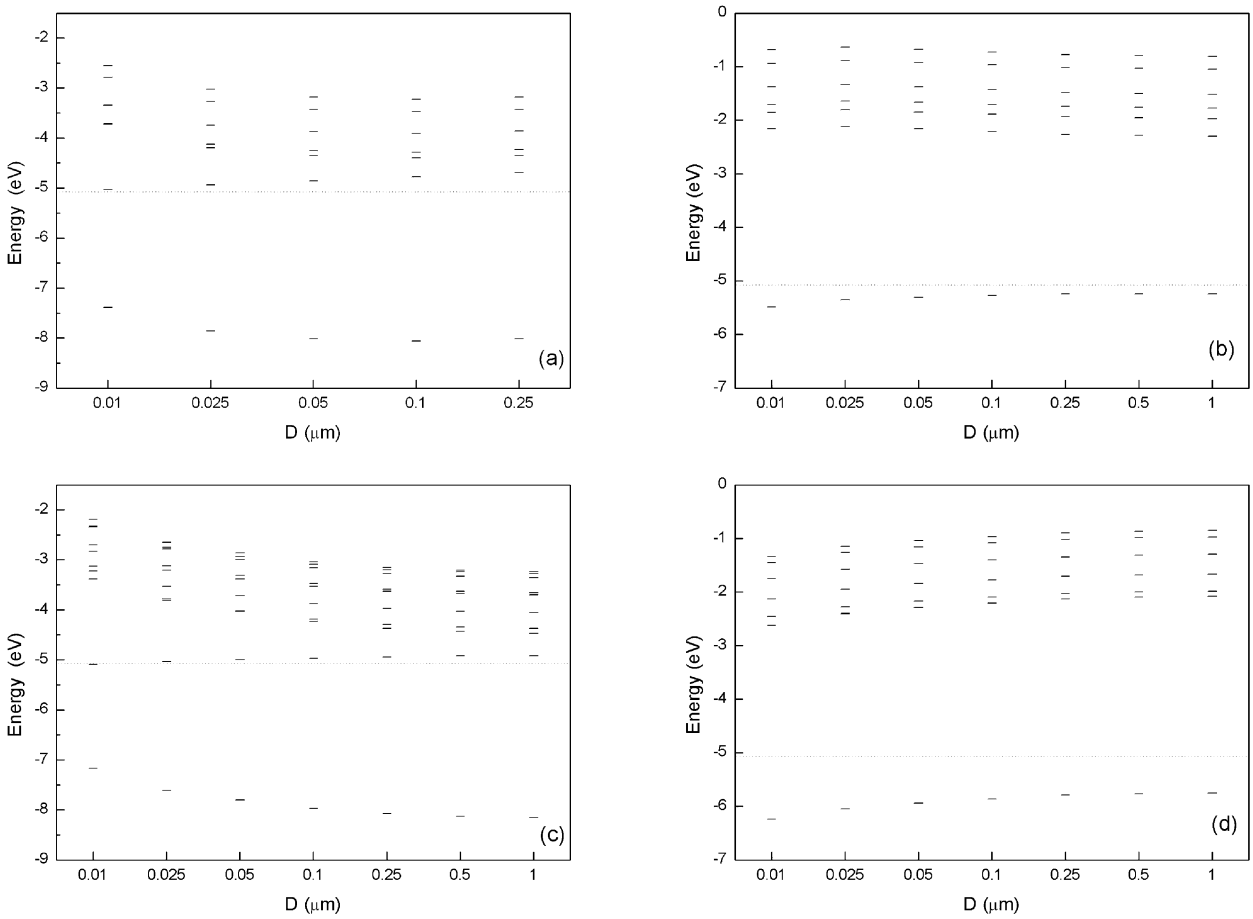

Figure 8. The energy levels of the apex subsystem: (a) open SWCNT in $E = 12.0$ V/μm; (b) open SWCNT in $E = 8.0$ V/μm; (c) capped SWCNT in $E = 12.0$ V/μm; (d) capped SWCNT in $E = 8.0$ V/μm.

simply referred to as emission probability) of electron with axial kinetic energy equal to the Fermi energy and is proportional to the emission current. The emission current of the CNT is estimated by

$$I = \nu q_{\text{exe}} T \tag{3}$$

where q_{exe} is the extra charge of the first layer atoms and ν is the collision frequency which can be estimated from the average kinetic energy of π^* electrons with $\nu = E_k(\pi^*)/h$, it is approximately 10^{14} Hz.[15,16]

The computed emission probabilities for the open and capped SWCNT under the applied macroscopic fields 12.0 and 8.0 V/μm are presented in parts a and b of Figure 3, respectively. The logarithmic scale is used for the probabilities. In the same applied macroscopic field and the same apex−anode distance, the emission probability of the open SWCNT is larger than that of the capped one. In the higher field (12.0 V/μm), the probability of the open SWCNT could be 1 order higher than that of the capped SWCNT. It should be related to the nonlinear behavior of the barrier height. We will come back to this point in subsection D.

Our calculated results confirm the anticipation that the emission current increases as the anode plate approaches the CNT. The emission probability increases rapidly with decreasing D, due to the barrier lowering and narrowing. To show the field dependence on emission current, we simulate the FE for $E =$ 10.0, 11.0, 12.0, 13.0, and 14.0 V/μm, with D fixed to be 0.1 and 1.0 μm. The currents are given in Figure 4a for the open SWCNT and Figure 4b for the capped SWCNT. The corresponding Fowler−Nordheim (FN) plots are given as insets.

With higher applied macroscopic field, the lowering of the barrier caused by field penetration should be more significant. Therefore the FN plots are obviously nonlinear, which is different from the FN theory.

C. Field Enhancement Factor. Denote the field at the steepest descent point of the barrier in the outer side of the barrier as E_s. The FEF of the present paper is defined as the ratio of E_s over the applied macroscopic field E, i.e., $\beta = E_s/E$. This definition reflects the thickness of the barrier. The simulation results for two values of E are presented in Figure 5. As expected, the thickness of the barrier is thinner in higher applied macroscopic field E. The thickness is decreasing with the separation D monotonously. As a consequence, the FEF β decreases as D increases. This effect occurs because, in the system configuration described, the FEF is a function of the apex−anode separation D. Therefore, if we consider a fixed value of applied macroscopic field, then the barrier field (i.e., the field that determines the tunneling barrier) becomes a function of the apex−anode separation.

If we used the same definition of applied macroscopic field as ref 5, then our $\beta_1 = E_s/E_1$ with $E_1 = V/D$ should have qualitatively the same behavior as β_1 of ref 5. Comparison shows that our simulations and those of Smith et al.[5,6] do exhibit the same qualitative trend, i.e., β_1 increases with D (Figure 6), even though the anode geometry is different in detail (their anode is not a plane).

In literature, the finite element method (FEM) is often used to obtain the electrostatic potential in large scale.[7] The field enhancement factor β (β_1) is calculated with the FEM. The results of various D under the fixed $E = 12.0$ V/μm are compared with those obtained via the quantum chemistry simulation in Table 1. In the FEM calculation, the open SWCNT is treated as a metallic empty cylinder with wall thickness 3.5 Å. The capped SWNT was treated as a metallic solid cylinder with a hemisphere cap. It was found that β (β_1) obtained via the FEM (the entries labeled by FEM) is significantly larger than the corresponding value obtained via the quantum chemistry simulation (the entries labeled quan). In the FEM calculation, the $\beta = E_s (L + D)/V$ and $\beta_1 = E_s D/V$, with E_s the classical steepest decreasing field on the outer side of the barrier (image potential has been included). The definition of β_1 coincides with that given in ref 7.

D. Barrier Height. The effective work function W_{eff} is related to the barrier height H via $W_{eff} = H - E_f$. The barrier height versus the anode distance D is given in Figure 7 for $E =$ 12.0 and 8.0 V/μm. For the same anode distance D, the barrier height for stronger applied macroscopic field ($E = 12.0$ V/μm) is lower than that of the weaker one ($E = 8.0$ V/μm). When the applied macroscopic field is fixed, in most cases the barrier height decreases as the anode approaches the SWCNT. But there is an exception: the capped SWCNT in $E = 12.0$ V/μm (squares in Figure 7). It is decreasing with D *increasing* peculiarly.

To explain this interesting exception, we plotted the energy levels of the apex subsystem in Figure 8 against the separation D. In Figure 8c for the capped SWCNT in $E = 12.0$ V/μm, one sees that an energy level sinks down the Fermi level in $D \sim 0.025$ μm. As a consequence, two more electrons will appear in the apex. They raise the potential energy of electron in the barrier region and give the unusual change of the barrier height as in Figure 7 (squares).

IV. Summary

Field electron emission of single-walled (5,5) carbon nanotubes 1.0 μm long with various anode distances has been simulated by a multiscale quantum chemistry method. The apex−vacuum electron potential energy barrier and the emission probability have been calculated. It is found that the steepest decreasing slope of the electron potential energy barrier near the apex (the local field) is decreasing; hence the field enhancement factor defined as the ratio of the local field over the applied macroscopic field is also decreasing, with increasing distance between the apex and anode, when the applied macroscopic field (defined as the ratio of the cathode−anode voltage over the cathode−anode distance) is fixed. With this condition, the emission current is also decreasing with increasing apex−anode separation. Our result is consistent with the experiment of Bonard et al.[22] The variation trend of the field enhancement factor against the anode separation is also consistent with refs 5, 6, and 7, but different definitions of the field enhancement factor should be distinguished carefully.

The simulation reveals the quantum mechanical origin of the nonlinear behavior of the potential energy barrier against the apex−anode separation. For the carbon nanotubes, the barrier height and barrier thickness, as the two most important features of field emission probability, incorporate quantum contributions which cannot be explained by the classical theory. As evidence, the present paper has shown that the barrier height (equivalently, effective work function) depends on both the applied field and the apex−anode separation. In the capped SWCNT with the field of 12.0 V/μm, we found that the barrier height increases as the apex−anode separation decreases. It indicates that an energy level crosses the Fermi energy level in certain separation.

Acknowledgment. The project is supported by the National Natural Science Foundation of China (Grant Nos. 10674182, 90103028, and 90306016) and National Basic Research Program of China (2007CB935500).

References and Notes

(1) Choi, W. B.; Chung, D. S.; Kang, J. H.; Kim, H. Y.; Jin, Y. W.; Han, I. T.; Lee, Y. H.; Jung, J. E.; Lee, N. S.; Park, G. S.; Kim, J. M. *Appl. Phys. Lett.* **1999**, *75*, 3129.

(2) de Jonge, N.; Lamy, Y.; Schoots, K.; Oosterkamp, T. H. *Nature* **2002**, *420*, 393.

(3) Semet, V.; Binh, V. T.; Vincent, P.; Guillot, D.; Teo, K. B. K.; Chhowalla, M.; Amaratunga, G. A. J.; Milne, W. I.; Legagneux, P.; Pribat, D. *Appl. Phys. Lett.* **2002**, *81*, 343.

(4) Harris, P. J. F. *Carbon Nanotubes and Related Structures*; Cambridge University Press: Cambridge and New York, 1999.

(5) Smith, R. C.; Carey, J. D.; Forrest, R. D.; Silva, S. R. P. *J. Vac. Sci. Technol., B* **2005**, *23* (2), 632.

(6) Smith, R. C.; Cox, D. C.; Silva, S. R. P. *Appl. Phys. Lett.* **2005**, *87*, 103112.

(7) Xu, Z.; Bai, X. D.; Wang, E. G. *Appl. Phys. Lett.* **2006**, *88*, 133107.

(8) de Heer, W. A.; Chatelain, A.; Ugarte, D. *Science* **1995**, *270*, 1179.

(9) Saito, Y.; Hamaguchi, K.; Nishino, T.; Hata, K.; Tohji, K. *Jpn. J. Appl. Phys., Part 2* **1997**, *36*, L1340.

(10) Bonard, J. M.; Salvetat, J. P.; Stockli, T.; Forra, L.; Chatelain, A. *Appl. Phys. A: Mater. Sci. Process.* **1999**, *69*, 245.

(11) Edgcombe, C. J.; Valdre, U. *J. Microsc.* **2001**, *203*, 188.

(12) Filip, V.; Nicolaescu, D.; Okuyama, F. *J. Vac. Sci. Technol., B* **2001**, *19*, 1016.

(13) Adessi, C. H.; Devel, M. *Phys. Rev. B* **2002**, *65*, 075418.

(14) Peng, Jie; Li, Zhibing; He, Chunshan; Chen, Guihua; Wang, Weiliang; Deng, Shaozhi; Xu, Ningsheng; Zheng, Xiao; Chen, GuanHua; Edgcombe, Chris J.; Forbes, Richard G. *J. Appl. Phys.* **2008**, *104*, 014310.

(15) Zheng, Xiao; Chen, GuanHua; Li, Zhibing; Deng, Shaozhi; Xu, Ningsheng *Phys. Rev. Lett.* **2004**, *92*, 106803.

(16) Peng, Jie; Li, Zhibing; He, Chunshan; Deng, Shaozhi; Xu, Ningsheng *Phys. Rev. B* **2005**, *72*, 235106.

(17) Chen, Guihua; Li, Zhibing; Peng, Jie; He, Chunshan; Wang, Weiliang; Deng, Shaozhi; Xu, Ningsheng *J. Phys. Chem. C* **2007**, *111* (13), 4939.

(18) Michael, J. S.; Dewar, Walter Thiel *J. Am. Chem. Soc.* **1977**, *99*, 4899.

(19) Yang, Weitao *Phys. Rev. Lett.* **1991**, *66*, 1438.

(20) Chen, Guihua; Wang, Weiliang; Peng, Jie; He, Chunshan; Deng, Shaozhi; Xu, Ningsheng; Li, Zhibing *Phys. Rev. B* **2007**, *76*, 195412.

(21) Froman, N.; Froman, P. O. *JWKB Approximation: Contributions to the theory*; North-Holland: Amsterdam, 1965.

(22) Bonard, J. M.; Maier, F.; Stockli, T.; Chatelain, A.; de Heer, W. A.; Salvetat, J. P.; Forro, L. *Ultramicroscopy* **1998**, *73*, 7.

JP810212G